IEEE Access
Multidisciplinary | Rapid Review | Open Access Journal

Received December 11, 2019, accepted January 2, 2020, date of publication January 6, 2020, date of current version January 14, 2020.

Digital Object Identifier 10.1109/ACCESS.2020.2964309

An Improved Multiport DC Power Flow Controller for VSC-MTDC Grids

WEN WU[1], XUEZHI WU[1,2], YUMING ZHAO[3], LUOCHENG WANG[4], (Student Member, IEEE), TIEFU ZHAO[4], (Senior Member, IEEE), AND LONG JING[1]

[1]National Active Distribution Network Technology Research Center, Beijing Jiaotong University, Beijing 100044, China
[2]Collaborative Innovation Center of Electric Vehicles, Beijing Jiaotong University, Beijing 100044, China
[3]Shenzhen Power Supply Company, Shenzhen 518000, China
[4]Electrical and Computer Engineering Department, Energy Production and Infrastructure Center, University of North Carolina at Charlotte, Charlotte, NC 28262, USA

Corresponding author: Xuezhi Wu (xzhwu@bjtu.edu.cn)

This work was supported by the China Southern Power Grid Company, Ltd., Science and Technology Project: Research and Application of Key Technologies of Integrated Energy System Based on DC under Grant 090000KK52180116.

ABSTRACT As a key device to facilitate power flow in the multi-terminal direct current (MTDC) transmission system, DC power flow controller (DCPFC) can effectively expand the power flow regulation area by implementing its multiport output functionality. In order to solve the coupling issue between the transmission line current and the capacitor voltage of the inter-line multiport DCPFC (M-DCPFC), an improved M-DCPFC with a partial power rated auxiliary DC/DC converter unit is proposed in this paper. It provides the advantages of power flow reversal, high adjustment flexibility and low port-expansion cost. Meanwhile, a generic control strategy is developed for the M-DCPFC with random number of the ports. Moreover, from the perspective of the transmission system, the proposed M-DCPFC is modeled as the equivalent series voltage source. Its power flow adjustment capability and its impact on the local voltage source converter (VSC) stations are investigated in detail in this paper. Lastly, to validate the effectiveness of the proposed M-DCPFC, it is first tested in the simulations of the MATLAB/Simulink and then deployed on an experiment platform. Both simulation and experimental results show that the proposed M-DCPFC can achieve stable power flow control in different conditions.

INDEX TERMS Multi-terminal direct current transmission system, DC power flow controller, multiport, power flow adjustment capability.

I. INTRODUCTION

With the shortage of traditional energy and the deterioration of the ecological environment, the widely utilization of green and clean energy has become an inevitable trend [1]. In order to ensure the efficient use of large-scale renewable sources, the transmission technology of multi-terminal direct current based on voltage source converter (VSC-MTDC) has become one of the main approaches to maintain the grid connection of the renewable energy [2], [3]. However, uncontrolled distribution of the power flow in the VSC-MTDC transmission system may cause line overload, unnecessary line loss and even damage the safe operation of the entire transmission system [4]. Therefore, maintaining the current on each transmission line in an optimized state is one of the key issues that VSC-MTDC transmission system must face and need to solve [5], [6].

In order to facilitate the power flow inside the VSC-MTDC transmission system, a conventional device known as the DC power flow controller (DCPFC) can be employed [7]. Since the power flow inside DC system can be controlled by either adjusting the resistance on the transmission line or regulating the DC voltage across the transmission line, the design approaches for the DCPFC can generally be classified into these two types, which are the resistance control type and the DC voltage control type [8]. 1) For the resistance control type DCPFC [9], [5], it has the advantages of simple structure and easy control. However, it can only have the equivalent resistance increased to regulate the power flow in one direction and will cause high system loss. Hence, it is usually not considered in the practical applications. 2) For the DC voltage control type DCPFC, according to the

The associate editor coordinating the review of this manuscript and approving it for publication was Zhu Han.

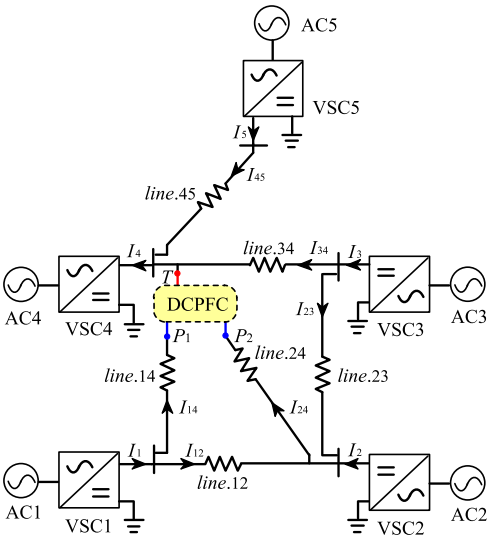

FIGURE 1. Diagram of the five-terminal VSC-MTDC transmission system with DCPFC.

implementation means of voltage control, it can be further divided into the DC transformer type [10]–[12] and the series voltage source type [13]–[20]. In comparison, the series voltage source type DCPFC can avoid the input and output sides of the DCPFC withstanding the system-level high voltage simultaneously, which provides the advantage of lower power level requirements of the device. Therefore, it has become a promising type of DCPFC candidate with more research attentions and better application prospects [16], [17].

By adopting the thyristor-based converter, a series voltage source type DCPFC topology is proposed in [13]. It can realize the bidirectional regulation of the power flow. But it needs to absorb energy from the AC grid, which makes the structure of this DCPFC complicated. To solve this problem, the concept of inter-line DCPFC (IDCPFC) is first proposed in [14], and several improved IDCPFC topologies are further investigated in [15]–[18]. This type of DCPFC has a fewer number of components and no interconnection with the AC grid, but it cannot realize the power flow reversal control. To address this issue, by increasing the amounts of DC capacitors and introducing coupled inductors, some novel types of IDCPFCs that can assist power flow reversal control are investigated in [7], [19]–[21]. In addition, by combining the modular multilevel converter (MMC) device, a MMC-based IDCPFC is proposed in [22]. However, it should be noted that the above mentioned DCPFCs are all two-port devices. As depicted in Figure 1, they can only control the power flow on single line (I_{14} or I_{24}), where the VSC 4 is set as DC voltage station, which is operating in the constant DC voltage control-mode; the VSC1, VSC2, VSC3 and VSC5 are set as power stations, which are operating in the constant power control-mode. If multiple power flow regulation of transmission lines are required to be coordinated, the multiport DCPFC (M-DCPFC) topology should be developed, and this is focus of this paper.

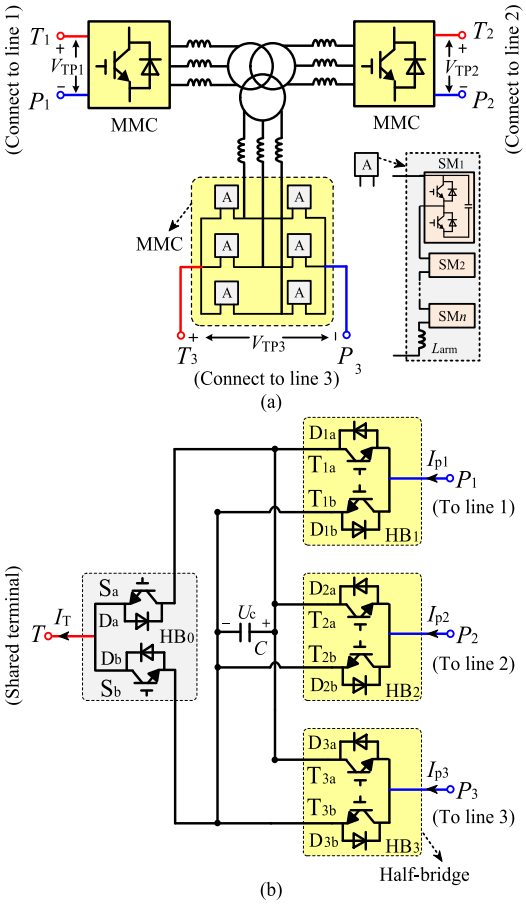

FIGURE 2. Topologies of the traditional M-DCPFC: (a) traditional M-DCPFC topology proposed in [23]; (b) previous inter-line M-DCPFC topology proposed in [25].

Currently, several studies on the M-DCPFC have been carried out, but they are still in their infancies. Inspired by the MMC-based IDCPFC proposed in [22], as shown in Figure 2(a), a MMC-based M-DCPFC topology is developed in [23]. Its main idea is to connect an equivalent DC voltage source in series with each transmission line separately through the different ports T_1P_1, T_2P_2 and T_3P_3. It has high adjustment flexibility, and the bidirectional control of the power flow can be realized. However, its multiport interface needs to be implemented by interconnecting the multi-winding transformer and MMCs, which results in high system cost, complicated system structure and inconvenient port-expansion. In addition, it cannot directly track the line current commands for power flow control, which adversely affects the control accuracy of the device. In [24], an inter-line M-DCPFC topology based on the insulated gate bipolar transistor (IGBT) half-bridge module is proposed, and its simplified topology is developed in [25], as shown in Figure 2(b). T and P are the terminals of the inter-line M-DCPFC, which are used for connecting the transmission lines. The common terminal T shared with the separate terminal P to constitute the different ports TP_1, TP_2 and TP_3. The structure is significantly simplified compared to the MMC-based M-DCPFC

topology presented in [23]. Besides, it can directly track the line current commands for power flow regulation with the higher control accuracy.

However, this simplified topology still contains some drawbacks. Its capacitor voltage U_c will be affected by the state of the line currents flowing through the capacitor, which cannot be controlled separately. This coupling issue between the line current and the capacitor voltage will cause the U_c to be varied when the power flow regulation command is changed, which may adversely affect the safe operation of the device. What is more, when the controlled line current I_{p1} is reduced to zero, it cannot continue charging the capacitor, which causes I_{p1} always staying in one polarity, thereby failing to realize the power flow reversal.

Based on the previous work in [25], by introducing a partial power rated auxiliary DC/DC converter unit, an improved M-DCPFC is proposed in this paper. It solves the coupling issue between the line current and the capacitor voltage of the previous inter-line M-DCPFC, which makes the M-DCPFC have higher adjustment flexibility and can realize the power flow reverse control. In addition, a generic control strategy is developed for the M-DCPFC with the random number of the ports. Moreover, from the perspective of the transmission system, the proposed M-DCPFC is modeled as the equivalent series voltage source. Its power flow adjustment capability and its impact on the local VSC stations are investigated in detail in this paper. The remainder of this paper is organized as follows: the topology and operation principle of the proposed M-DCPFC are analyzed in Section II. Section III describes the control algorithm. The capacity design and power flow control characteristics of the M-DCPFC are discussed in Section IV. The simulation and experimental results are presented in Sections V and VI respectively. Finally, conclusions are drawn in Section VII.

II. TOPOLOGY AND OPERATION PRINCIPLE OF THE PROPOSED M-DCPFC

A. TOPOLOGY

The structure of the proposed M-DCPFC is shown in Figure 3. For an n-port M-DCPFC, it consists of $n + 1$ IGBT half-bridges (HBs) and an auxiliary DC/DC converter unit composed by m identical DC/DC modules. With no interconnection with the AC grid and following the design concept presented in [26], as shown in Figure 3(b), the DC/DC converter unit adopts the input series output parallel (ISOP) configuration which can take power from the DC bus of the transmission system directly.

Where, S_a/S_b and D_a/D_b are the upper/lower switch and anti-parallel diode of HB_0 respectively. T_{ia}/T_{ib} ($i = 1, 2 \ldots n$) and D_{ia}/D_{ib} are the upper/lower switch and anti-parallel diode of HB_i respectively. Terminals T, P_i and S are defined as the output terminal, input terminal and auxiliary terminal respectively. The common terminal T shared with the separate terminal P_i to constitute n different output ports TP_i of the M-DCPFC. I_{Pi} are the different controlled line currents

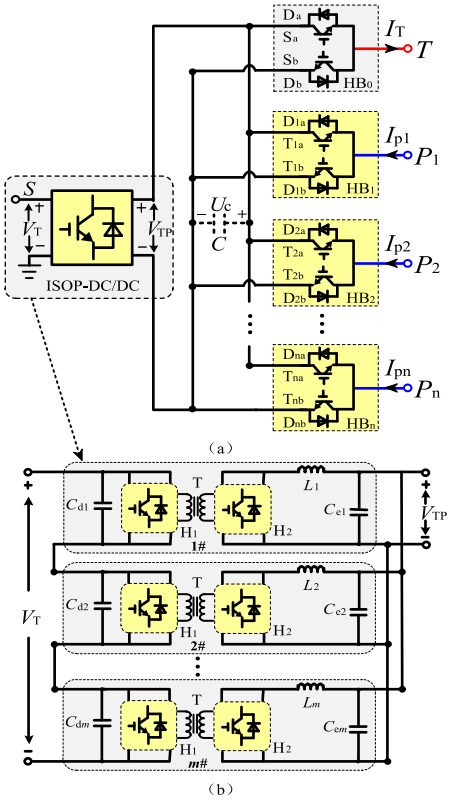

FIGURE 3. Topology of the proposed M-DCPFC: (a) topology of the M-DCPFC; (b) topology of the ISOP DC/DC converter unit.

flowing into the device; I_T is the total current flowing out of the controller. In addition, it should be noted that the DC capacitor C depicted in Figure 3(a) is the equivalent capacitor of the output side of the ISOP DC/DC converter unit. For the convenience of illustration and subsequent analysis, we virtualized it at the location shown.

B. CONNECTION TO THE MTDC

The following work actually can be applied to any VSC-MTDC transmission system. For this study, a typical five-terminal VSC-MTDC transmission system [25] is adopted as an example to carry out the related analysis.

As depicted in Figure 4, a three-port proposed M-DCPFC is deployed. Its terminals T and S are connected to the bus convergence point of the different power stations, that is, the DC bus side of VSC4. In addition, its terminals P_1,P_2 and P_3 are connected to the different controlled transmission lines *line*.14, *line*.24 and *line*.34, respectively. Different with the DCPFC shown in Figure 2, the M-DCPFC can regulate the line currents I_{14} and I_{24} at the same time through the expansion of the port TP_3, so the overall power flow control of this five-terminal transmission system can be achieved. In addition, it should be noted that the power consumed on terminal S for the inner voltage V_{TP} regulation is drown directly from the transmission system. However, the required value of V_{TP} is much smaller than the rated DC bus voltage V_T.

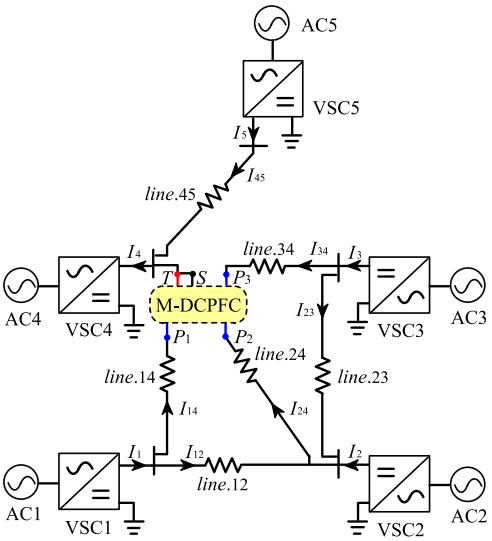

FIGURE 4. Diagram of the five-terminal VSC-MTDC transmission system accessed with three-port proposed M-DCPFC.

Thus, the impact of this power consumption is negligible to the overall transmission system. This point is further analyzed in detail in Section IV.

C. OPERATION PRINCIPLE

For facilitating the subsequent analysis, the positive direction of the line currents I_{Pi} and I_T is defined as the current flowing into the terminals P_i and T. In addition, assuming that the output voltage of the ISOP DC/DC converter unit is stable at V_{TP}, the voltage of the capacitor C corresponds equal to V_{TP}.

1) LINE CURRENT DIRECTIONS ARE POSITIVE

Figure 5 shows two typical switching modes of the proposed M-DCPFC when the directions of the controlled line currents are positive.

As depicted in Figure 5(a), when the upper switch S_a of HB_0 is turned-on and the lower switches T_{ib} ($i = 1, 2, 3$) of $HB_1 \sim HB_3$ are also turned-on, it can be easily observed that the output voltage of each port of the M-DCPFC is $V_{TP1} = U_c$; $V_{TP2} = U_c$; $V_{TP3} = U_c$, respectively. On the other hand, when the upper switch of HB_0 is kept turned-on, the lower switches T_{ib} of $HB_1 \sim HB_3$ are turned-off, it can be seen that the output voltage of each port of the M-DCPFC is changed to $V_{TP1} = 0$; $V_{TP2} = 0$; $V_{TP3} = 0$, respectively, where the specific conduction diagram under this switching mode is shown as Figure 5(b).

Further promotion can be found that when the directions of the controlled line currents are positive, by keeping the upper switch S_a of HB_0 is turned-on and controlling the on/off state of the lower switches T_{ib} of $HB_1 \sim HB_3$, the adjustable DC voltage $V_{TP1} = D_1U_c$; $V_{TP2} = D_2U_c$; $V_{TP3} = D_3U_c$ can be obtained at each output port of the M-DCPFC, respectively. Where, $D_1 \sim D_3$ are the duty ratios of the lower switches T_{ib} of $HB_1 \sim HB_3$, respectively. By adjusting the duty ratios $D_1 \sim D_3$, the $V_{TP1} \sim V_{TP3}$ can be regulated independently

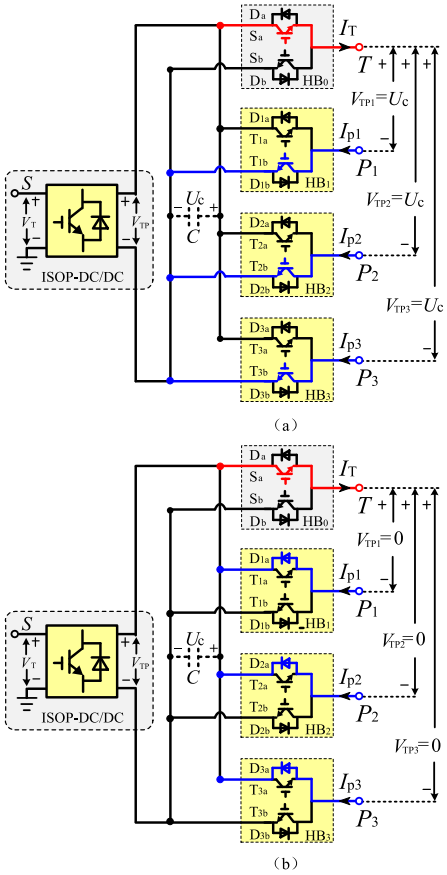

FIGURE 5. Typical switching modes of the proposed M-DCPFC when the controlled line current directions are positive: (a) switching mode when T_{ib} are turned-on; (b) switching mode when T_{ia} are turned-off.

and then the power flow control on each transmission line can be realized with these series voltage sources.

2) LINE CURRENT DIRECTIONS ARE NEGATIVE

Figure 6 shows two typical switching modes of the proposed M-DCPFC when the directions of the controlled line currents are negative.

As shown in Figure 6(a), when the lower switch S_b of HB_0 is turned-on and the upper switches T_{ia} of $HB_1 \sim HB_3$ are also turned-on, it can be seen that the output voltage of each port of the M-DCPFC is $V_{TP1} = -U_c$; $V_{TP2} = -U_c$; $V_{TP3} = -U_c$, respectively. On the other hand, when the lower switch S_b of HB_0 is kept turned-on, the upper switches T_{ia} of $HB_1 \sim HB_3$ are turned-off, it can be found that the output voltage of each port of the M-DCPFC is changed to $V_{TP1} = 0$; $V_{TP2} = 0$; $V_{TP3} = 0$, respectively, where the specific conduction diagram under this switching mode is shown as Figure 6(b).

Similarly, further promotion can be found that when the directions of the controlled line currents are negative, if the upper and lower switches of each half-bridge are in a complementary conduction state, by keeping the lower switch S_b of HB_0 is turned-on and controlling the on/off state of the upper switches T_{ia} of $HB_1 \sim HB_3$, the adjustable DC

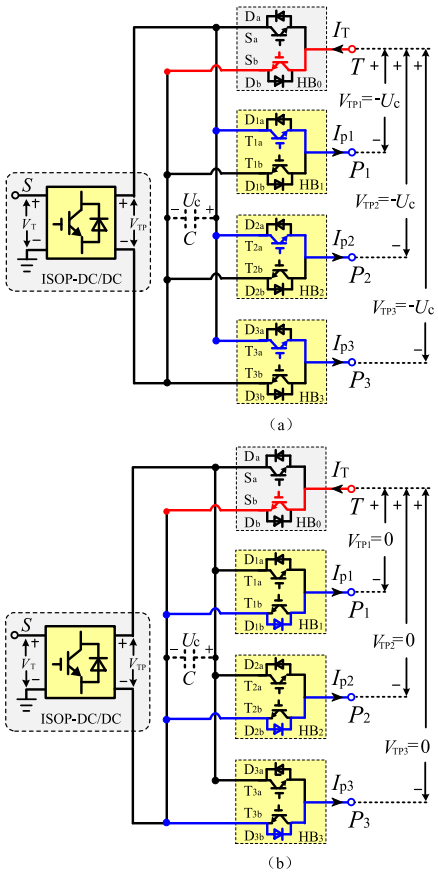

FIGURE 6. Typical switching modes of the proposed M-DCPFC when the controlled line current directions are negative: (a) switching mode when T_{ia} are turned-on; (b) switching mode when T_{ia} are turned-off.

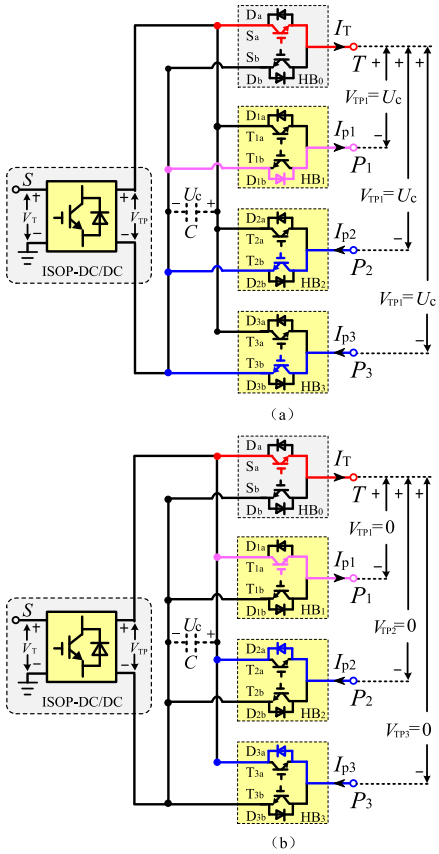

FIGURE 7. Typical switching modes of the proposed M-DCPFC when the controlled line current directions are different: (a) switching mode when T_{ib} are turned-on; (b) switching mode when T_{ib} are turned-off.

voltage V_{TP1} =-(1-D_1)U_c; V_{TP2} =-(1-D_3)U_c; V_{TP3} =-(1-D_3)U_c can be obtained at each output port of the M-DCPFC, respectively.

3) LINE CURRENT DIRECTIONS ARE DIFFERENT

When the current directions of the controlled lines are different, take the current I_{p1} is negative and the currents I_{p2},I_{p3} are positive as an example. Under this condition, the current I_T flowing out of the controller may be positive or negative. Assuming that current I_T is still negative, the two typical switching modes of the proposed M-DCPFC under this condition can be shown as Figure 7.

Comparing Figure 7 with Figure 5, it can be found that when the direction of the line current I_{p1} is changed, the adjustable DC voltage $V_{TP1} = D_1U_c$; $V_{TP2} = D_2U_c$; $V_{TP3} = D_3U_c$ can also be obtained at each output port of the M-DCPFC, respectively. Similarly, the power flow control of the transmission system can be realized by adjusting the duty ratios $D_1 \sim D_3$.

Besides, when the current I_T is positive or other controlled line currents are reversed, some other switching modes of the M-DCPFC will be developed accordingly. However, the working principles are basically similar to those above, thereby not described in detail.

III. DESIGN OF THE CONTROL STRASTEGY

In the previous analysis, a three-port M-DCPFC was taken as the example, and its basic working principle is analyzed in detail. In this section, the control method is developed to be applicable to the M-DCPFC with random number of the ports.

A. OVERALL CONTROL FRAME

The control strategy of the M-DCPFC can be divided into two parts:

1) One is the control of ISOP DC/DC converter unit, which completes the auxiliary control of the capacitor voltage U_c, and the conventional three-loop control strategy [26], [27] is adopted in this study;
2) The other one is the control of the parallel half-bridge unit, which completes the specific regulations of the transmission line currents. It is discussed in the part *B* of this section.

B. CONTROL OF THE PARALLEL HALF-BRIDGE UNIT

Combined with the previous analysis in part *C* of Section II, the control method of the parallel half-bridge unit can be developed as follows:

1) When the current I_T is negative, regardless of the directions of the controlled line currents I_{Pi}, by keeping the upper switch S_a of HB_0 turned on and controlling the duty ratio D_i of the lower switches T_{ib} of HB_i, it can be ensured that the equivalent adjustable DC voltage sources $V_{TPi} = D_iU_c$ are connected in series to the corresponding controlled transmission lines;
2) When the current I_T is positive, regardless of the directions of the controlled line currents I_{Pi}, by keeping the lower switch S_b of HB_0 turned on and identically controlling the duty ratios of the lower switches T_{ib} of HB_i, it can be ensured that the equivalent adjustable DC voltage sources $V_{TPi} = -(1\text{-}D_i)U_c$ are connected in series to the corresponding controlled lines.

Considering that when the VSC stations of the transmission system are operating in the steady state, the total current $(I_{p1}+I_{p2}+\ldots+I_{pn})$ flowing through the M-DCPFC is stable. Thus, for n controlled transmission lines, current control for all of them can be achieved by tracking current regulation commands on n-1 lines. The remaining transmission line can be set as the slack line and the switches in its connected half-bridge only need to operate at the fixed duty ratio. Taking the transmission line which is connected to HB_1 as the slack branch as an example, the control block diagram of the parallel half-bridge unit of the n-port M-DCPFC can be shown as Figure 8.

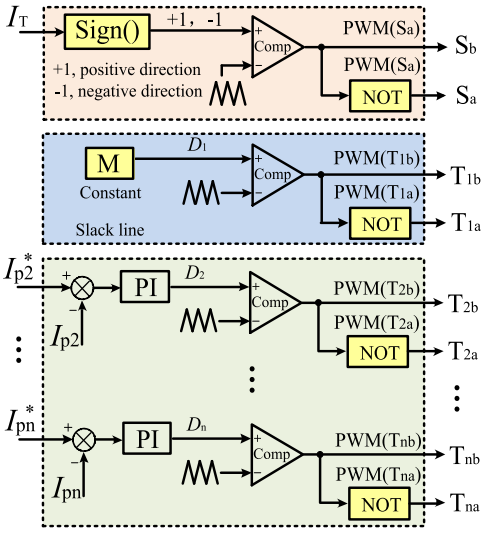

FIGURE 8. Block diagram of the control strategy.

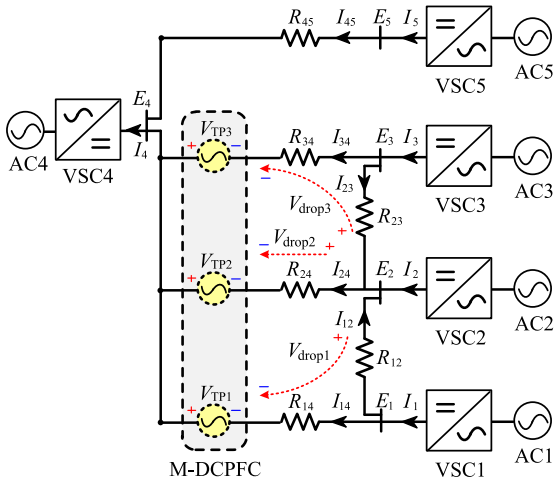

FIGURE 9. Equivalent circuit of the transmission system accessed with the proposed M-DCPFC.

C. DSEIGN OF THE SLACK LINE

According to Figure 4, the equivalent circuit of the transmission system with the proposed M-DCPFC can be obtained as Figure 9. I_j and E_j (j = 1, 2, . . ., 5) are the DC side current and voltage of each corresponding VSC station respectively; R_{ij} (i, j = 1, 2, . . ., 5; i < j) is the resistance of each corresponding transmission line.

Assuming the power flow regulation command of the controlled lines is $[I_{14}*, I_{24}*, I_{34}*]$, the drop voltage across the line resistances of each parallel branch can be calculated as:

$$\begin{cases} V_{\text{drop1}} = I_{14}^* R_{14} + \left(I_{14}^* - I_1\right) R_{12} \\ V_{\text{drop2}} = I_{24}^* R_{24} \\ V_{\text{drop3}} = I_{34}^* R_{34} + \left(I_{34}^* - I_3\right) R_{23} \end{cases} \tag{1}$$

where, it can be approximated that $I_1 = P_1/E_4$; $I_2 = P_2/E_4$ and $I_3 = P_3/E_4$. Solving equation (1), assume that:

$$V_{\text{drop1}} \geq V_{\text{drop2}} \geq V_{\text{drop3}} \tag{2}$$

In addition, the equation (3) can be obtained according to the KVL:

$$V_{\text{drop1}} - V_{\text{TP1}} = V_{\text{drop2}} - V_{\text{TP2}} = V_{\text{drop3}} - V_{\text{TP3}} \tag{3}$$

It is easy to know that the required compensation voltage for *line*.14 is $(V_{\text{drop1}}\text{-}V_{\text{drop3}}) = (V_{\text{TP1}}\text{-}V_{\text{TP3}})$ and for *line*.24 is $(V_{\text{drop2}}\text{-}V_{\text{drop3}}) = (V_{\text{TP2}}\text{-}V_{\text{TP3}})$. In order to minimize the output voltage of each port of the M-DCPFC, *line*.34 can be selected as the slack line and V_{TP3} is set to 0. Therefore, the line in the parallel branch which the drop voltage is minimized can be selected as the slack line, and in order to ensure the output voltage of the port in slack line is 0, the duty cycle D of slack line should be set to 0 when the current I_T is negative and set to 1 when the current I_T is positive.

IV. CAPACITY DESIGN AND POWER FLOW CONTROL CHARACTERISTICS OF THE M-DCPFC

A. POWER FLOW CONTROL CHARACTERISTICS

According to Figure 9, the related system matrix equation can be obtained:

$$\begin{bmatrix} R_{14} & 0 & 0 & 0 & 0 & 0 \\ 0 & R_{24} & 0 & 0 & 0 & 0 \\ 0 & 0 & R_{34} & 0 & 0 & 0 \\ 0 & 0 & 0 & R_{45} & 0 & 0 \\ 0 & 0 & 0 & 0 & R_{12} & 0 \\ 0 & 0 & 0 & 0 & 0 & R_{23} \end{bmatrix}$$

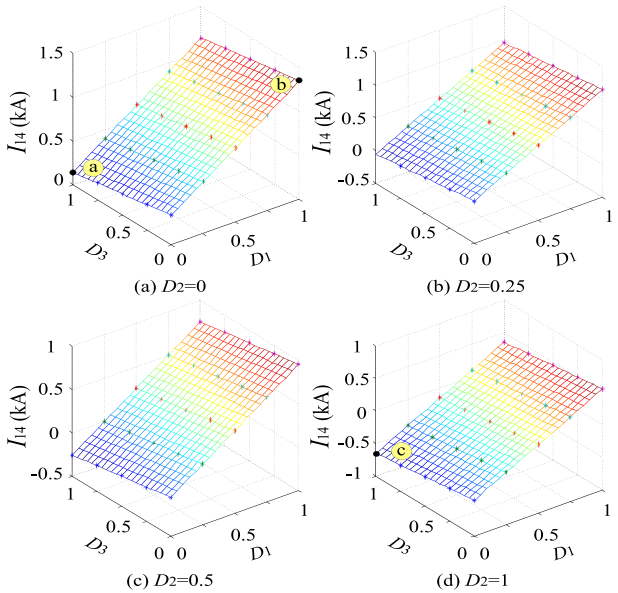

FIGURE 10. 3-D curves of the transmission line current I_{14}.

TABLE 1. VSC station parameters of the transmission system.

Converter station	Control mode	Command
VSC1	Constant power	P_1=40MW
VSC2	Constant power	P_2=50MW
VSC3	Constant power	P_3=30MW
VSC4	Constant DC voltage	V_4=100kV
VSC5	Constant power	P_5=40MW

$$*\mathbf{I}_{ij} = \begin{bmatrix} E_1 - E_4 \\ E_2 - E_4 \\ E_3 - E_4 \\ E_5 - E_4 \\ E_1 - E_2 \\ E_2 - E_3 \end{bmatrix} + \begin{bmatrix} V_{TP1} \\ V_{TP1} \\ V_{TP1} \\ 0 \\ 0 \\ 0 \end{bmatrix} \tag{4}$$

$\mathbf{I}_{ij}$ is the relevant matrix of transmission line currents, where $\mathbf{I}_{ij} = [I_{14}\ I_{24}\ I_{34}\ I_{45}\ I_{12}\ I_{23}]$. In addition, since the VSC1∼VSC3 are operating as constant power output nodes, the following equation can be obtained:

$$\begin{bmatrix} E_1 & 0 & 0 & 0 & E_1 & 0 \\ 0 & E_2 & 0 & 0 & -E_2 & E_2 \\ 0 & 0 & E_3 & 0 & 0 & -E_3 \\ 0 & 0 & 0 & E_5 & 0 & 0 \end{bmatrix} * I_{ij} = \begin{bmatrix} P_1 \\ P_2 \\ P_3 \\ P_5 \end{bmatrix} \tag{5}$$

Specifically, the main parameters of each VSC station and transmission line are shown in Tables 1 and 2, respectively.

Assuming that the capacitor voltage U_c is stable at 4kV, then combining equations (4), (5) and the specific parameters of the transmission system shown in Tables 1 and 2, the following results can be calculated by adopting the control variates method:

1) When D_2 respectively takes the value 0; 0.25; 0.5 and 1, the 3-D curves of the controlled line currents I_{14} and I_{34} varied with D_1 and D_3 are shown in Figures 10 and 11, respectively;

TABLE 2. Line parameters of the transmission system.

Line	Length/ km	Resistance/ Ω	Inductance/ mH	Capacitance/ uF
line.14	200	2.0	80	240
line.24	100	1.0	40	120
line.34	300	3.0	120	360
line.45	150	1.5	60	180
line.35	100	1.0	40	120
line.12	120	1.2	48	144
line.23	100	1.0	40	120

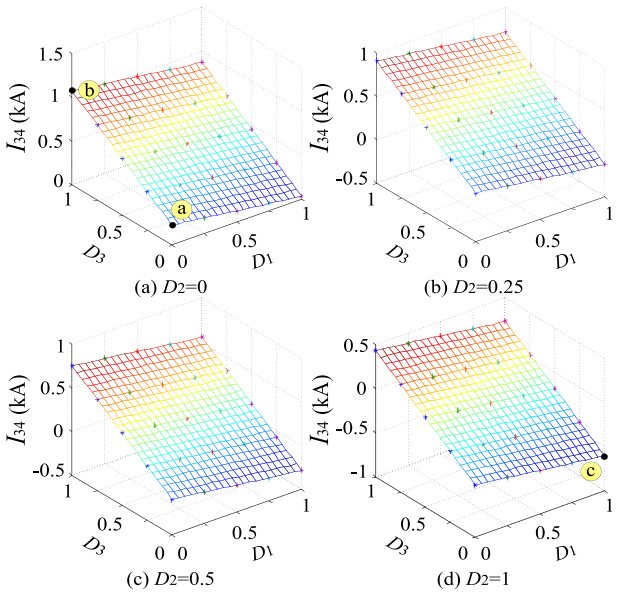

FIGURE 11. 3-D curves of the transmission line current I_{34}.

2) When D_2 respectively takes the value 0 and 1, the 3-D curves of the DC side voltage of each transmitting converter station varied with D_1 and D_3 are shown in Figure 12;
3) When D_2 respectively takes the value 0; 0.25; 0.5 and 1, the 3-D curves of the power of receiving converter station varied with D_1 and D_3 are shown in Figure 13.

Based on the above calculated results, when the M-DCPFC proposed in the paper participates in the system power flow control, the following related conclusions can be obtained:

1) ***Power flow adjustment capability*:** combining Figures 10 and 11, standardizing the line currents I_{14} and I_{34} with their rated values, as shown in equations (6) and (7), it can be found that the controlled line currents I_{14} and I_{34} can be adjusted within the wide range of [−1.89pu, 3.93pu] and [−2.64pu, 4.67pu], respectively;

$$\begin{cases} \varepsilon(I_{14\_max}) = \dfrac{I_{14}(\max)}{I_{14}(\text{rated})} = \dfrac{I_{14}(b)}{I_{14}(a)} = 3.93\text{pu} \\ \varepsilon(I_{14\_min}) = \dfrac{I_{14}(\min)}{I_{14}(\text{rated})} = \dfrac{I_{14}(c)}{I_{14}(a)} = -1.89\text{pu} \end{cases} \tag{6}$$

$$\begin{cases} \varepsilon(I_{34\_max}) = \dfrac{I_{34}(\max)}{I_{34}(\text{rated})} = \dfrac{I_{34}(b)}{I_{34}(a)} = 4.67\text{pu} \\ \varepsilon(I_{34\_min}) = \dfrac{I_{34}(\min)}{I_{34}(\text{rated})} = \dfrac{I_{34}(c)}{I_{34}(a)} = -2.64\text{pu} \end{cases} \tag{7}$$

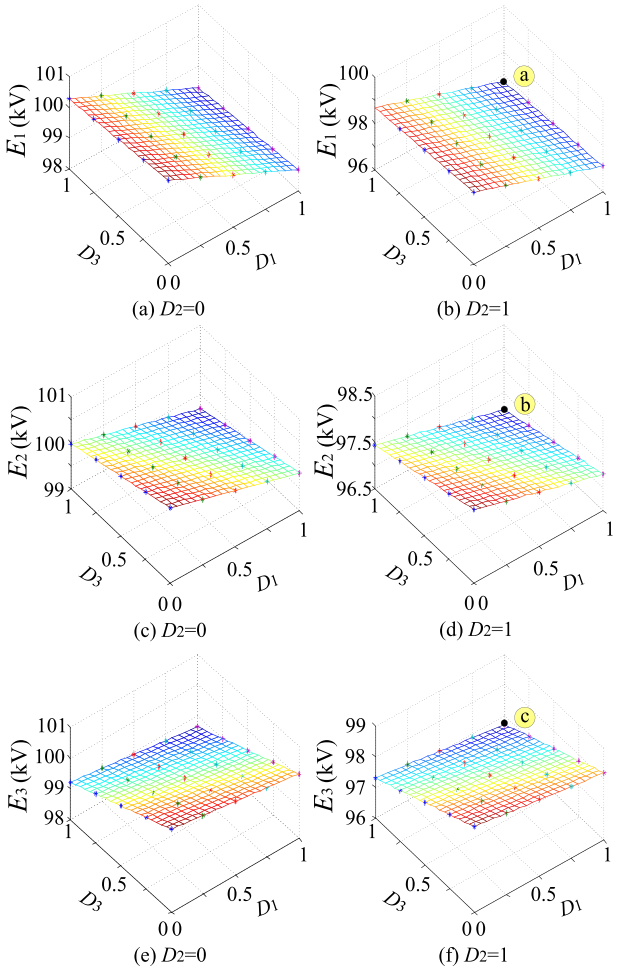

FIGURE 12. 3-D curves of the DC voltages of transmitting converter stations VSC1 to VCS3.

2) ***Influence on the transmitting converter station*:** since the transmitting converter station operates in the constant power control-mode, the variation of its DC side voltage is mainly investigated. As shown in Figure 12, affected by the voltage drop across the line resistance and the M-DCPFC, the DC side voltage of each transmitting converter station will be slightly lower than the rated DC bus voltage. However, in the process of regulating power flow by the proposed M-DCPFC, the fluctuations of the DC side voltage of each transmitting converter station are not obvious compared to the rated DC bus voltage. Among them, as shown in equation (8), the maximum fluctuations of the E_1, E_2 and E_3 are about 3.29%, 3.26% and 3.28%, respectively, all within 4%;

$$\begin{cases} \varepsilon(E_1) = \dfrac{E_{\text{rated}} - E_1(\text{min})}{E_{\text{rated}}} = \dfrac{E_4 - E_1(\text{a})}{E_4} = 3.29\% \\ \varepsilon(E_2) = \dfrac{E_{\text{rated}} - E_2(\text{min})}{E_{\text{rated}}} = \dfrac{E_4 - E_1(\text{b})}{E_4} = 3.26\% \\ \varepsilon(E_3) = \dfrac{E_{\text{rated}} - E_2(\text{min})}{E_{\text{rated}}} = \dfrac{E_4 - E_1(\text{c})}{E_4} = 3.28\% \end{cases} \tag{8}$$

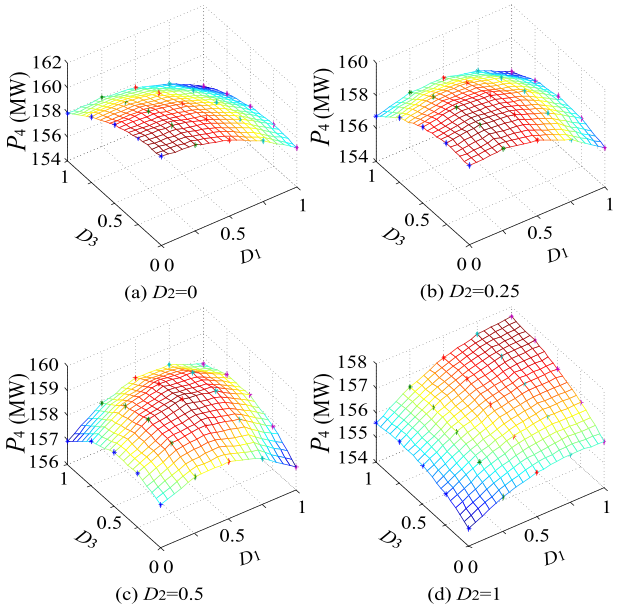

FIGURE 13. 3-D curves of the power of receiving converter station VSC4.

3) ***Influence on the receiving converter station*:** since the receiving converter station operates in the constant DC voltage control-mode, its power variation is mainly investigated. As shown in Figure 13, due to the energy consumption on M-DCPFC for power flow control, it will cause partial power loss of the transmission system. But the maximum acquired power from the transmission system for the M-DCPFC is about 5.8 MW, and this value can also be considered as the rated power design requirement of the M-DCPFC, which is about 3.7% of the transmission system rated capacity.

In concluded, we can found that the proposed M-DCPFC can achieve the power flow control in bidirectional and wide range, and it has relatively low power design requirement compared to the transmission system rated capacity. In addition, it has little influence on the local VSC stations, which basically does not affect the normal operation of the entire transmission system.

B. CAPACITY DESIGN

It is easy to know that the maximum required output voltage of the ports of the M-DCPFC is the maximum required voltage of the capacitor C. Therefore, the rated capacitor voltage U_c can be designed according to the maximum required output voltage of the ports of the M-DCPFC.

Assume that the regulation requirements of I_{14}, I_{24}, and I_{34} are $[I_{14\text{min}}, I_{14\text{max}}]$, $[I_{24\text{min}}, I_{24\text{max}}]$ and $[I_{34\text{min}}, I_{34\text{max}}]$, respectively. As shown in Figure 9, $(I_{14} + I_{24} + I_{34})$ can be approximately considered to be stable when the VSCs are under steady state operation. Therefore, when the two currents of I_{14}, I_{24}, and I_{34} are all reduced to the minimum, the other one is necessarily increased to the maximum. This is also the most extreme current regulation condition. At this

time, the required output voltage of the M-DCPFC will be the maximum.

Similar to the calculation method in part *C* of Section III, when the power flow control command is $[I_{14\max}, I_{24\min}, I_{34\min}]$, the drop voltage across the line resistances of each parallel branch can be calculated as:

$$\begin{cases} V_{\text{drop1}}|_{I_{14}=I_{14\max}} = I_{14\max}R_{14} + (I_{14\max} - I_1)\,R_{12} \\ V_{\text{drop2}}|_{I_{14}=I_{14\max}} = I_{24\min}R_{24} \\ V_{\text{drop3}}|_{I_{14}=I_{14\max}} = I_{34\min}R_{34} + (I_{34\min} - I_3)\,R_{23} \end{cases} \tag{9}$$

The maximum required output voltage of the ports of the M-DCPFC under this condition can be obtained as:

$$V_{\text{TPmax1}} = V_{drop(\max 1)} - V_{drop(\min 1)} \tag{10}$$

where:

$$\begin{cases} V_{\text{drop(max1)}} = \text{Max}(V_{\text{drop1}}|_{I_{14}=I_{14\max}}, \\ \qquad V_{\text{drop2}}|_{I_{14}=I_{14\max}}, V_{\text{drop3}}|_{I_{14}=I_{14\max}}) \\ V_{\text{drop(min1)}} = \text{Min}(V_{\text{drop1}}|_{I_{14}=I_{14\max}}, \\ \qquad V_{\text{drop2}}|_{I_{14}=I_{14\max}}, V_{\text{drop3}}|_{I_{14}=I_{14\max}}) \end{cases} \tag{11}$$

Similarly, when the power flow control commands are $[I_{14\min}, I_{24\max}, I_{34\min}]$ and $[I_{14\min}, I_{24\min}, I_{34\max}]$, the maximum required output voltages of the ports of the M-DCPFC can be calculated as V_{TPmanx2} and V_{TPmax3} respectively. Take the maximum of V_{TPmanx1}, V_{TPmanx2} and V_{TPmax3}:

$$V_{\text{TPmax}} = \text{Max}\,(V_{\text{TPmax1}}, V_{\text{TPmax2}}, V_{\text{TPmax3}}) \tag{12}$$

This voltage V_{TPmax} is the maximum required voltage of the ports of the M-DCPFC, that is, the rated voltage of the capacitor. The rated capacitor voltage and the maximum current flowing through the ISOP DC/DC can be used to design the capacity $P_{\text{M-DCPFC}}$ of M-DCPFC, where $P_{\text{M-DCPFC}} = V_{\text{TPmax}}I_{\text{T}}$. The design method of the M-DCPFC with other number of the ports can be developed in the same way.

V. SIMULATION STUDIES

In order to verify the proposed M-DCPFC, the five-terminal VSC-MTDC transmission system as shown in Figure 4 and a more complex transmission system as shown in Figure 14(b) are developed in the MATLAB/Simulink. The parameters of each converter station are shown in Table 1; the parameters of the transmission line are shown in Table 2.

A. VERIFICATION OF THE THREE-PORT M-DCPFC

1) CASE1: BALANCE THE LINE CURRENTS

After the system starts normally, the capacitor voltage U_{c} is set to 4kV and the M-DCPFC is inserted to the system with bypass-state, that is, the output voltage of each port is zero. At $t = 1$s, balance the line currents of *line*.14, *line*.24 and *line*.34.

The performance of the M-DCPFC in this case is shown in Figure 15(a)-(c). It can be observed that the transmission line currents are running stable after the system is started up, as shown in Figure 15(a), and the corresponding current

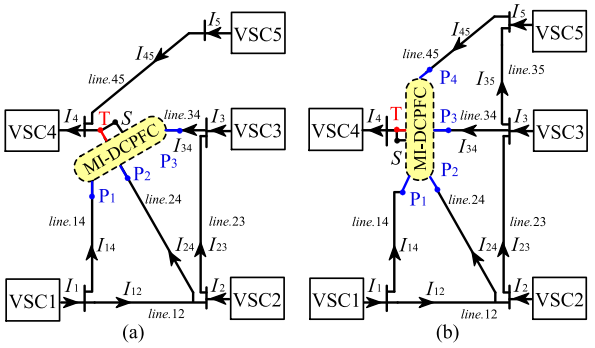

FIGURE 14. Five-terminal VSC-MTDC transmission systems: (a) with three-port M-DCPFC; (b) with four-port M-DCPFC.

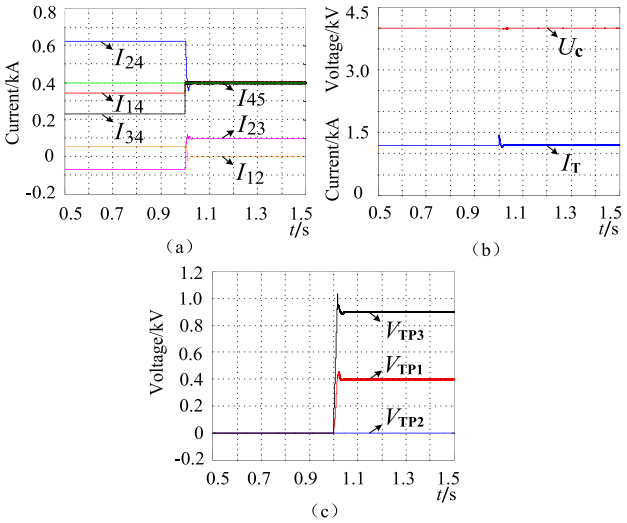

FIGURE 15. Simulation results of steady state regulation: (a) line currents; (b) capacitor voltage and output current of the M-DCPFC; (c) average port output voltage of the M-DCPFC.

values are $I_{12} = 0.06$kA; $I_{14} = 0.35$kA; $I_{23} = -0.07$kA; $I_{24} = 0.62$kA; $I_{34} = 0.23$kA and $I_{45} = 0.40$kA, respectively. When the power flow control command is adjusted at $t = 1$s, the controlled line currents I_{14} and I_{34} all quickly respond to the command value 0.4kA, as shown in Figure 15(a); and the average output voltage of each port of the M-MCPFC is changed accordingly, as shown in Figure 15(c). In addition, as shown in Figure 15(b), besides a slight transient impact at the power flow adjustment moment, the capacitor voltage and output current of M-DCPFC can always maintain stable operation.

2) CASE2: REVERSE THE LINE CURRENTS

The initial operating conditions of the system are consistent with the case 1. At $t = 1$s, reverse the line currents of *line*.14 and *line*.34 are reversed simultaneously, i.e., control $I_{14} = -0.35$kA and $I_{34} = -0.23$kA.

The performance of the M-DCPFC in this case is shown in Figure 16(a)-(c). It can be seen that when the power flow control command is adjusted at $t = 1$s, the average output

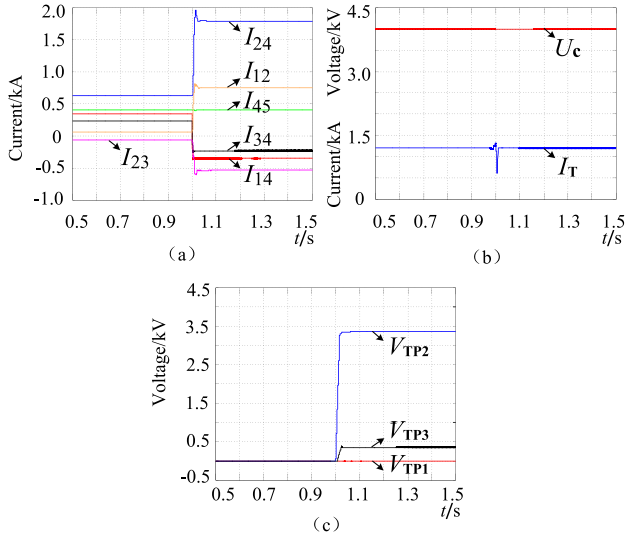

FIGURE 16. Simulation results of power flow reversal: (a) line currents; (b) capacitor voltage and output current of the M-DCPFC; (c) average port output voltage of the M-DCPFC.

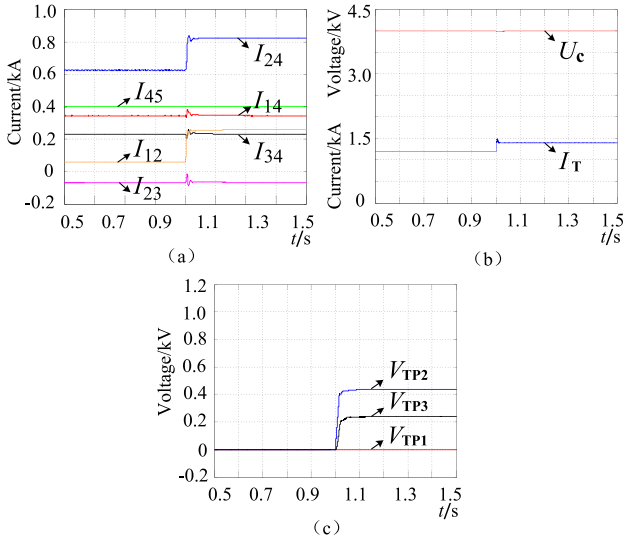

FIGURE 17. Simulation results when the output power of VSC1 is stepped up: (a) line currents; (b) capacitor voltage and output current of the M-DCPFC; (c) average port output voltage of the M-DCPFC.

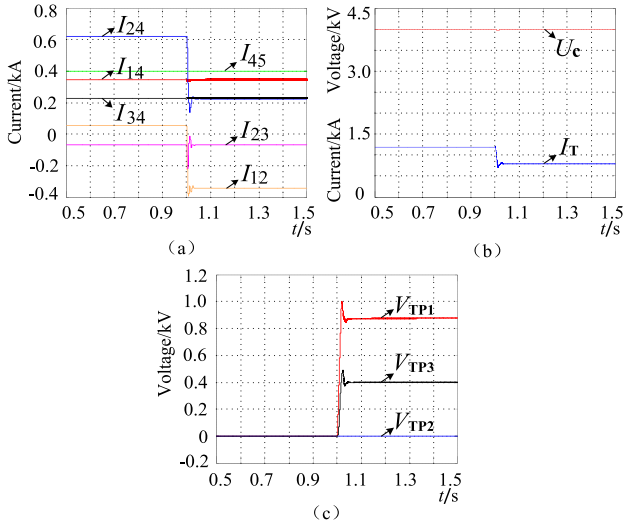

FIGURE 18. Simulation results when the output power of VSC1 is lost: (a) line currents; (b) capacitor voltage and output current of the M-DCPFC; (c) average port output voltage of the M-DCPFC.

voltage of each port of the M-DCPFC is correspondingly changed to different value, as shown in Figure 16(c), and the controlled line currents I_{14} and I_{34} are also all quickly responding to the command values -0.35kA and -0.23kA, respectively, as shown in Figure 16(a). Similarly, as shown in Figure 16(b), besides a transient impact at the power flow adjustment moment, the capacitor voltage and output current of M-DCPFC also always maintain stable operation.

3) CASE3: KEEP LINE CURRENTS STABLE WHEN VSC1 OUTPUT POWER IS STEPPED UP

The initial operating conditions of the system are consistent with the case 1. At $t = 1$s, the output power of VSC1 is stepped from 40MW to 60MW, but keep the line currents of *line*.14 and *line*.34 all stable.

The simulation results in this case are shown in Figure 17(a)-(c). It can be seen that when the output power of VSC1 station is stepped up at $t = 1$s, the total current of the transmission line, i.e., the output current of the M-DCPFC is correspondingly increased, as shown in Figure 17(b). However, with the control of M-DCPFC, the controlled line currents I_{14} and I_{34} can all operate stable with their original value, as shown in Figure 17(a). In addition, as shown in Figure 17(b), the capacitor voltage of M-DCPFC always maintains stable operation before and after the VSC1 output power step up.

4) CASE4: KEEP LINE CURRENTS STABLE WHEN VSC1 OUTPUT POWER IS LOST

The initial operating conditions of the system are consistent with the case 1. At $t = 1$s, the output power of VSC1 is lost, but control the line currents of *line*.14 and *line*.34 all remain constant.

The simulation results in this case are shown in Figure 18(a)-(c). Similarly, the controlled line current I_{14} and I_{34} can all operate stable with the original value with the control of M-DCPFC, as shown in Figure 18(a). The output current of the M-DCPFC is correspondingly decreased, and the capacitor voltage of the M-DCPFC always keeps stable operation, as shown in Figure 18(b).

B. VERIFICATION OF THE FOUR-PORT M-DCPFC

After the system starts normally, the capacitor voltage U_c is set to 4kV and the M-DCPFC is inserted to the system with bypass-state. At $t = 1$s, the following three different conditions are verified respectively.

1) Case1: I_{14} is reduced to 0.05kA; I_{24} and I_{45} are increased to 0.7kA and 0.5kA, respectively;

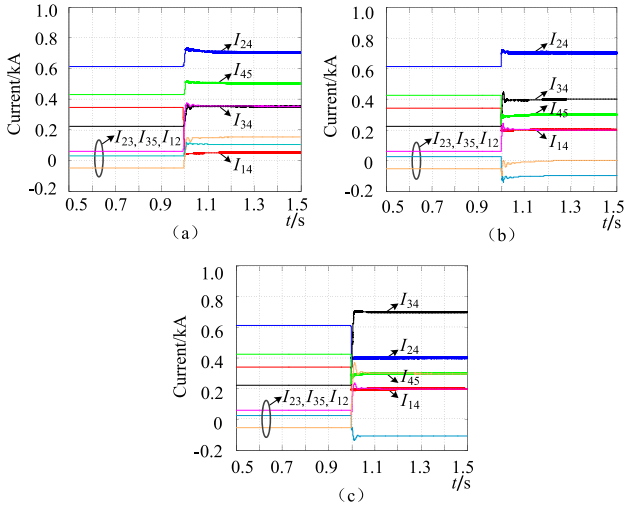

FIGURE 19. Simulation results of the four-port M-DCPFC: (a) line currents under case 1; (b) line currents under case 2; (c) line currents under case 3.

2) Case2: I_{14} and I_{45} are reduced to 0.2kA and 0.3kA, respectively; I_{24} is increased to 0.7kA;
3) Case3: I_{14}, I_{45} and I_{24} are reduced to 0.2kA, 0.3kA and 0.4kA, respectively.

The main simulation results are shown in Figure 19(a)-(c). It can be observed that the line currents are running stable after the system is started up, and the corresponding current values are $I_{12} = 0.07$kA; $I_{14} = 0.33$kA; $I_{23} = -0.06$kA; $I_{24} = 0.62$kA; $I_{34} = 0.21$kA; $I_{35} = 0.03$kA and $I_{45} = 0.43$kA, respectively. When the power flow control command is changed at $t = 1.0$s, the controlled lines can all quickly track the corresponding power flow control commands, and then maintain stable operation.

VI. EXPERIMENTS

To further validate the proposed M-DCPFC topology and control strategy, as shown in Figure 20, a down-scale five-terminal VSC-MTDC transmission system is built in the laboratory, and its topologies is consistent with the simulation, as shown in Figure 14.

Each power module in the Units 1 to 3 has half-bridge and full-bridge two different topology mode to be selected. Specifically, Unit1 and Uuit3 adopt the full-bridge topology mode to form the ISOP DC/DC converter unit of the M-DCPFC, and Unit2 adopt the half-bridge topology mode to compose the parallel half-bridge unit of the M-DCPFC. VSC1∼VSC5 adopt the ITECH programmable digital power IT series (each ITECH power source has two independent output channels), and its specific working mode is shown in Table 3. The experimental line parameters are shown in Table 4.

A. VERIFICATION OF THE THREE-PORT M-DCPFC

1) SYSTEM TEST

The performance of the platform with three-port M-DCPFC under normal operation state is shown in Figure 21. It can

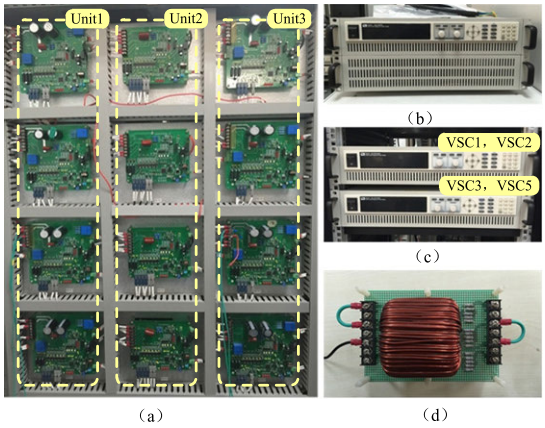

FIGURE 20. Photograph of the experiment platform: (a) prototype of the M-DCPFC; (b) VSC4; (c) VSCs1-3 and 5; (d) line impedance module.

TABLE 3. Experiment VSC station parameters.

Converter node	Operation mode	Command
VSC1	Current mode	I_1=4A
VSC2	Current mode	I_2=5A
VSC3	Current mode	I_3=3A
VSC4	Voltage mode	V_4=80V
VSC5	Current mode	I_5=4A

TABLE 4. Experiment line parameters.

Line	Resistance/Ω	Inductance/mH
line.14	2.0	4.0
line.24	1.0	3.0
line.34	3.0	5.0
line.45	1.5	4.0
line.35	1.0	3.0
line.12	1.2	3.0
line.23	1.0	3.0

be seen that the system is running stable when it is started up. In addition, the measured values of each line current are about $I_{14} = 3.5$A; $I_{24} = 6.4$A; $I_{34} = 2.4$A; $I_{45} = 4$A; $I_{12} = 0.6$A and $I_{23} = -0.7$A, respectively.

2) EXPERIMENTAL RESULTS

In order to facilitate the comparison and verification of the simulation results, the same cases as the simulation are tested in the experiment, respectively.

Case 1: after the system starts normally, the capacitor voltage is set to 15V and the M-DCPFC is inserted to the system with bypass-state; at t_1, control the line currents of *line*.14, *line*.24 and *line*.34 are averaged. The experimental results in this case are shown in Figure 22 (a)-(b). It can be observed that when the power flow control command is adjusted at t_1, the controlled line currents I_{14} and I_{34} all quickly respond to the command value 4A, as shown in Figure 22(a); and as shown in Figure 22(b), besides a slight transient impact

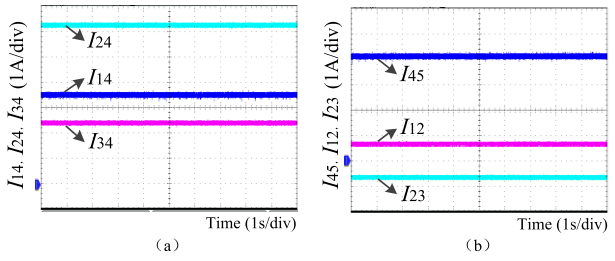

FIGURE 21. Experimental results of three-port M-DCPFC under normal operation state: (a) line currents I_{14}, I_{24}, I_{34}; (b) line currents I_{45}, I_{12}, I_{23}.

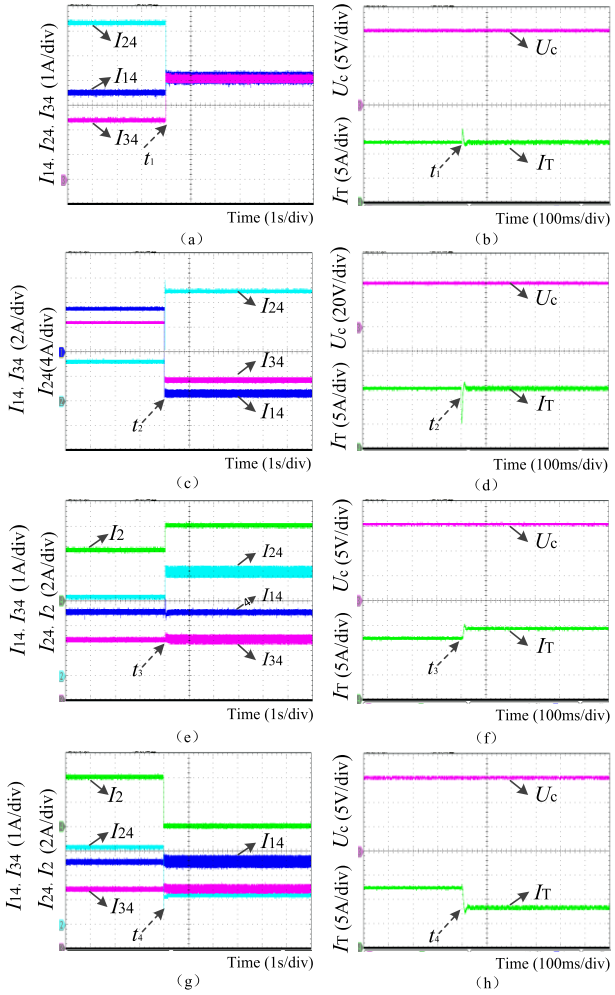

FIGURE 22. Experimental results of the three-port M-DCPFC: (a) line currents under case1; (b) Capacitor voltage and output current of the M-DCPFC under case 1; (c) line currents under case2; (d) Capacitor voltage and output current of the M-DCPFC under case 2; (e) line currents under case3; (f) Capacitor voltage and output current of the M-DCPFC under case 3; (g) line currents under case4; (h) Capacitor voltage and output current of the M-DCPFC under case 4.

at the power flow adjustment moment, the capacitor voltage and output current of M-DCPFC can always maintain stable operation.

Case 2: after the system starts up normally, the capacitor voltage is set to 36V and the M-DCPFC is inserted to the system with bypass-state; at t_2, control the line currents I_{14} and I_{34} are reversed simultaneously. The experimental results in this case are shown in Figure 22 (c)-(d). It can be seen that when the power flow control command is adjusted at t_2, I_{14} and I_{34} can also quickly respond to the command value -3.5A and -2.4A, respectively, as shown in Figure 22(c). Similarly, besides a transient impact at the power flow adjustment moment, the capacitor voltage and output current of M-DCPFC can always maintain stable operation, as shown in Figure 22(d).

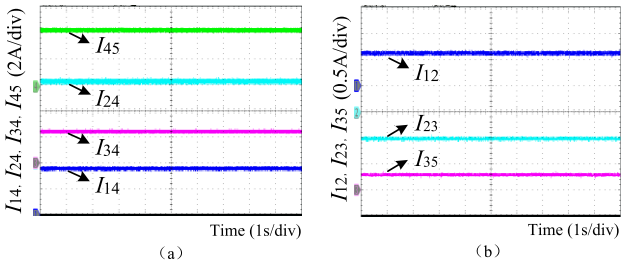

FIGURE 23. Experimental results of the four-port M-DCPFC under normal operation state: (a) line currents I_{14}, I_{24}, I_{34}, I_{45}; (b) line currents I_{45}, I_{12}, I_{23}.

Cases 3 and 4: The initial operating conditions of the system are consistent with the *case 1*. In *Case 3*, the VSC1 output current I_1 step from 4A to 6A at t_3; in *Case 4*, the VSC1 output current I_1 is down from 4A to 0 at t_4. However, we all control the line currents I_{14} and I_{34} remain constant at t_3 and t_4. The related experimental results are shown in Figure 22 (e)-(h). It can be observed that the line currents of the system will be slightly disturbed when the output power of VSC1 is abrupt, but the controlled line currents I_{14} and I_{34} can all quickly stable in their original 3.5A and 2.3A, respectively.

B. VERIFICATION OF THE FOUR-PORT M-DCPFC

1) SYSTEM TEST

The performance of the platform with four-port M-DCPFC under normal operation state is shown in Figure 23. It can be seen that the system is running stable when it is started up. In addition, the measured values of each line current are about $I_{14} = 3.4$A; $I_{24} = 6.3$A; $I_{34} = 2.4$A; $I_{45} = 4.3$A; $I_{12} = 0.6$A; $I_{23} = -0.6$A and $I_{35} = 0.3$A, respectively.

2) EXPERIMENTAL RESULTS

In order to facilitate the comparison and verification of the simulation results, the same cases as the simulation are tested in the experiment, respectively.

1) Case1: I_{14} is reduced to 0.5A; I_{24} and I_{45} are increased to 7A and 5A, respectively;
2) Case2: I_{14} and I_{45} are reduced to 2A and 3A, respectively; I_{24} is increased to 7A;
3) Case3: I_{14}, I_{45} and I_{24} are reduced to 2A, 3A and 4A, respectively.

The main experimental results are shown in Figure 24(a)-(c). It can be observed that when the power flow control command is changed, the controlled lines can

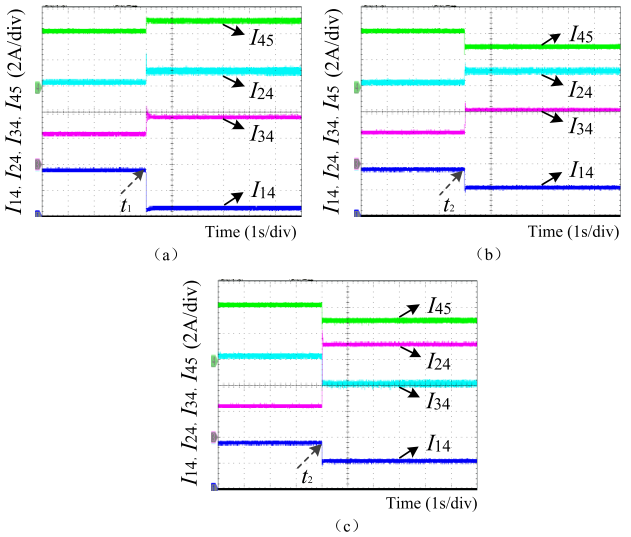

FIGURE 24. Experimental results of the four-port M-DCPFC: (a) line currents under case1; (b) line currents under case2; (c) line currents under case3.

all quickly track the corresponding power flow control commands, and then maintain stable operation.

Concluding the above simulation and experimental results, it can be found that the simulation and experimental results are basically consistent, which shows that the proposed M-DCPFC can achieve effective power flow control under different power flow adjustment requirements.

VII. CONCLUSION

The DC power flow control issue in VSC-MTDC transmission system is investigated in this paper. The main works and contributions can be summarized as:

1) An improved M-DCPFC is proposed, which has the following three main features: i) it solves the coupling issue between the transmission line current and the capacitor voltage of the previous M-DCPFC, which makes the M-DCPFC have higher adjustment flexibility and can help to realize the power flow reversal; ii) its port-expansion can be achieved by only adding the low voltage low cost half-bridge modules; iii) it can directly track the line current commands for power flow regulation with the high control accuracy.
2) A generic control strategy for the M-DCPFC with random number of the ports is designed. In addition, by establishing the equivalent circuit of the transmission system and combining with the actual example, the system operation characteristics are analyzed in detail. It reveals that the proposed M-DCPFC can achieve bidirectional and wide range power flow control with low rated power design requirement and has little impact on the operation of the local VSC stations.
3) Two 5-terminal VSC-MTDC transmission systems are developed in the MATLAB/Simulink and the experiment platform, respectively. The different conditions are verified, and the results show the effectiveness of the M-DCPFC.

Considering that ISOP DC/DC has some implementation difficulties in the high-voltage applications, so the M-DCPFC proposed in this paper is more suitable for medium voltage DC system. Developing the M-DCPFC suitable for high-voltage large-capacity DC system and fully exploiting the control potential of M-DCPFC, achieving introduces active damping assistance into the transmission line to help fault isolation are the next research directions.

REFERENCES

[1] J. Li, G. Konstantinou, H. R. Wickramasinghe, J. Pou, X. Wu, and X. Jin, "Impact of circulating current control in capacitor voltage ripples of modular multilevel converters under grid imbalances," *IEEE Trans. Power Del.*, vol. 33, no. 3, pp. 1257–1267, Jun. 2018.
[2] F. Yan, P. Wang, X.-P. Zhang, J. Xie, X. Li, C. Tang, and Z. Zhao, "Coordinated start-up control and inter-converter oscillations damping for MMC-HVDC grid," *IEEE Access*, vol. 7, pp. 65093–65102, 2019.
[3] H. Kim, J. Kang, J. W. Shim, J. Beerten, D. Van Hertem, H.-J. Jung, C.-K. Kim, and K. Hur, "Exploiting redundant energy of MMC–HVDC to enhance frequency response of low inertia AC grid," *IEEE Access*, vol. 7, pp. 138485–138494, 2019.
[4] S. Balasubramaniam, J. Liang, and C. Ugalde-Loo, "An IGBT based series power flow controller for multi-terminal HVDC transmission," in *Proc. Int. Univ. Power Eng. Conf.*, Cluj-Napoca, Romania, 2014, pp. 1–6.
[5] D. Jovcic, M. Hajian, H. Zhang, and G. Asplund, "Power flow control in DC transmission grids using mechanical and semiconductor based DC/DC devices," in *Proc. IET Int. Conf. AC DC Power Transmiss.*, Birmingham, U.K., 2012, pp. 1–6.
[6] Q. Mu, J. Liang, Y. Li, and X. Zhou, "Power flow control devices in dc grids," in *Proc. IEEE Power Energy Soc. Gen. Meeting*, San Diego, CA, USA, 2012, pp. 1–7.
[7] W. Chen, X. Zhu, L. Yao, X. Ruan, Z. Wang, and Y. Cao, "An interline DC power-flow controller (IDCPFC) for multiterminal HVDC system," *IEEE Trans. Power Del.*, vol. 30, no. 4, pp. 2027–2036, Aug. 2015.
[8] S. Wang, J. Guo, and C. Li, "Coordination of DC power flow controllers and AC/DC converters on optimizing the delivery of wind power," *IET Renew. Power Gener.*, vol. 10, no. 6, pp. 815–823, Sep. 2015.
[9] Q. Mu, J. Liang, Y. Li, and X. Zhou, "Power flow control devices in DC grids," in *Proc. IEEE Power Energy Soc. Gen. Meeting*, San Diego, CA, USA, Jul. 2012, pp. 1–7.
[10] K. Natori, H. Obara, K. Yoshikawa, B. Hiu, and Y. Sato, "Flexible power flow control for next-generation multi-terminal DC power network," in *Proc. IEEE Energy Convers. Congr. Expo.*, 2014, pp. 778–784.
[11] S. Kenzelmann, A. Rufer, and D. Dujic, "High frequency operation of a DC/AC/DC system for HVDC applications," *IEEE Trans. Power Electron.*, vol. 29, no. 8, pp. 4017–4115, Jan. 2015.
[12] S. Kenzelmann, A. Rufer, D. Dujic, F. Canales, and Y. R. De Novaes, "Isolated DC/DC structure based on modular multilevel converter," *IEEE Trans. Power Electron.*, vol. 30, no. 1, pp. 89–98, Jan. 2015.
[13] E. Veilleux and B.-T. Ooi, "Multiterminal HVDC with thyristor power-flow controller," *IEEE Trans. Power Del.*, vol. 27, no. 3, pp. 1205–1212, Jul. 2012.
[14] C. Barker and R. Whitehouse, "A current flow controller for use in HVDC grids," in *Proc. IET Int. Conf. AC DC Power Transmiss.*, Birmingham, U.K., 2012, pp. 1–5.
[15] N. Deng, P. Wang, X.-P. Zhang, G. Tang, and J. Cao, "A DC current flow controller for meshed modular multilevel converter multiterminal HVDC grids," *CSEE Power Energy Syst.*, vol. 1, no. 1, pp. 43–51, Mar. 2015.
[16] H. Y. Diab, M. I. Marei, and S. B. Tennakoon, "Reduced switch count topology of current flow control apparatus for MTDC grids," *J. Power Electron.*, vol. 16, no. 5, pp. 1743–1751, Sep. 2016.
[17] J. Sau-Bassols, E. Prieto-Araujo, and O. Gomis-Bellmunt, "Modeling and control of an interline current flow controller for meshed HVDC grids," *IEEE Trans. Power Del.*, vol. 32, no. 1, pp. 11–22, Feb. 2017.
[18] J. Sau-Bassols, E. Prieto-Araujo, O. Gomis-Bellmunt, and F. Hassan, "Series interline DC/DC current flow controller for meshed HVDC grids," *IEEE Trans. Power Del.*, vol. 33, no. 2, pp. 881–891, Apr. 2018.
[19] Y. Cao, L. Yao, and B. Yang, "A novel DC power flow controller for VSC-MTDC system," in *Proc. IET Int. Conf. Rene. Power Gener.*, Beijing, China, 2015, pp. 1–6.

[20] G. Ning, W. Chen, and X. Zhu, "A novel interline DC power flow controller for meshed HVDC grids," in *Proc. IEEE Conf. Energy Convers. Congr. Expo.*, Milwaukee, WI, USA, 2016, pp. 1–7.
[21] W. Chen, X. Zhu, L. Yao, G. Ning, Y. Li, Z. Wang, W. Gu, and X. Qu, "A novel interline DC power-flow controller (IDCPFC) for meshed HVDC grids," *IEEE Trans. Power Del.*, vol. 31, no. 4, pp. 1719–1727, Aug. 2016.
[22] M. Ranjram and P. W. Lehn, "A three-port power flow controller for HVDC grids," in *Proc. 9th Int. Conf. Power Electron.*, Seoul, South Korea, 2015, pp. 1–5.
[23] M. Ranjram and P. W. Lehn, "A multiport power-flow controller for DC transmission grids," *IEEE Trans. Power Del.*, vol. 31, no. 1, pp. 389–396, Feb. 2016.
[24] H. Y. Diab, M. I. Marei, and S. B. Tennakoon, "Operation and control of an insulated gate bipolar transistor-based current controlling device for power flow applications in multi-terminal high-voltage direct current grids," *IET Power Electron.*, vol. 9, no. 2, pp. 305–315, Feb. 2016.
[25] W. Wu, X. Wu, L. Jing, and J. Yin, "Investigate on a simplified multi-port interline DC power flow controller and its control strategy," *Energies*, vol. 12, no. 13, pp. 2480–2508, Jun. 2019.
[26] H. T. Zhang, L. Jing, and X. Z. Wu, "Power flow control scheme for multiport power electronics transformers," *IET High Voltage*, vol. 3, no. 4, pp. 255–262, Dec. 2018.
[27] W. Chen, K. Zhuang, and X. B. Ruan, "A input-series-and output- parallel-connected inverter system for high-input-voltage applications," *J. Power Electron.*, vol. 24, no. 9, pp. 2127–2137, Sep. 2009.

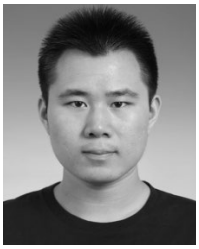

WEN WU received the B.S. degree in electrical engineering from Guangdong Ocean University, Zhanjiang, China, in 2014, and the M.S. degree in electrical engineering from Beijing Jiaotong University, Beijing, China, in 2017, where he is currently pursuing the Ph.D. degree with the Department of Electrical Engineering. His current research interests include modular multilevel converters, power electronics for high voltage direct current applications, and dc grids.

XUEZHI WU received the B.S. and M.S. degrees in electrical engineering from Beijing Jiaotong University, Beijing, China, in 1996 and 1999, respectively, and the Ph.D. degree in electrical engineering from Tsinghua University, Beijing, in 2002. He is currently an Associate Professor with the Department of Electrical Engineering, Beijing Jiaotong University, Beijing. His current research interests include micro grids, wind power generation systems, power converters for renewable generation systems, power quality, and motor control.

YUMING ZHAO received the B.S. and Ph.D. degrees in electrical engineering from Tsinghua University, Beijing, China, in 2001 and 2006, respectively. He is currently a Senior Engineer (Professor Level) of Shenzhen Power Supply Company. His current research interests include medium voltage direct current and low voltage direct current system design, and control and protect technology.

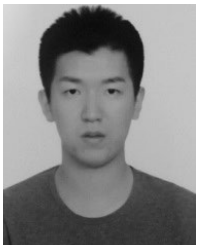

LUOCHENG WANG received the B.S. degree in electrical engineering from the University of Connecticut, Storrs, CT, USA, in 2014, and the M.S. degree in electrical and computer engineering from Cornell University, Ithaca, NY, USA, in 2016. He is currently pursuing the Ph.D. degree in electrical and computer engineering with the University of North Carolina at Charlotte, Charlotte, NC, USA. His current research interests include the advanced control of power converters and electrical drives, model predictive control, reliability in power electronics, grid-integration of renewable energy systems, and inductive power transfer.

TIEFU ZHAO received the B.S. and M.S. degrees in electrical engineering from Tsinghua University, Beijing, China, in 2003 and 2005, respectively, and the Ph.D. degree in electrical engineering from North Carolina University, Raleigh, NC, USA, in 2010. He is currently an Assistant Professor of electrical and computer engineering and an Associate of the Energy Production and Infrastructure Center (EPIC), University of North Carolina at Charlotte, Charlotte, NC. His current research interests include solid state transformer and solid state circuit protection, wireless power transfer, micro-grid and renewable energy integration, wide band-gap device applications, and power electronics reliability.

LONG JING received the B.S., M.S., and Ph.D. degrees in electrical engineering from Beijing Jiaotong University, Beijing, China, in 2000, 2002, and 2008, respectively. He is currently an Associate Professor with the Department of Electrical Engineering, Beijing Jiaotong University, Beijing. His current research interests include modular multilevel converters, dc grids, power electronics for high voltage direct current applications, and power converters for renewable generation systems.